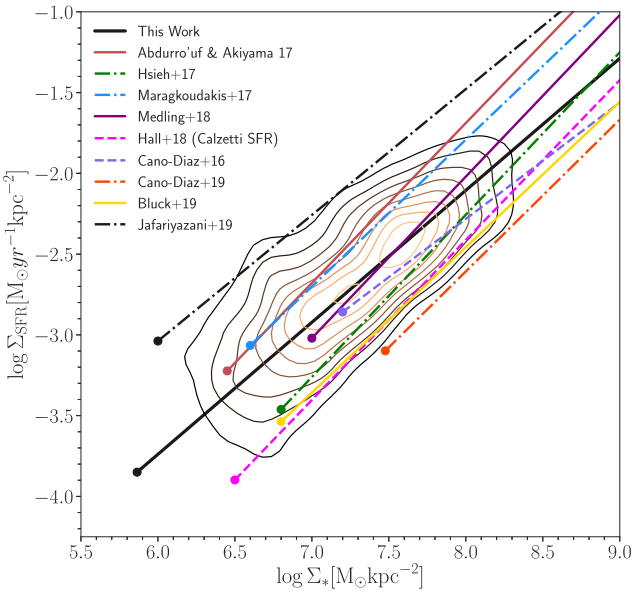

Figure 8. A comparison between our results (black-to-yellow contours encircling from 80 to 10 per cent of our data points, fitted by the solid black line) and a sample of resolved MS relations from the literature, respectively, with slopes reported in Table 2.. Each relation, which has been converted to a Chabrier (2003) IMF, and re-scaled to $z = 0$ (as described in the text), starts from the sensitivity limit reported in the study (or, if not, estimated from the relative data).

Table 2. Summary of the slopes quoted in the text, with associated SFR tracer.

Reference	Slope	SFR tracer
Cano-Díaz et al. (2016)	0.72	Hα
Abdurro'uf (2017)	0.99	SED fitting
Hsieh et al. (2017)	1.00	Hα
Maragkoudakis et al. (2017)	0.91	3.6 μm or 8.0 μm
Hall et al. (2018)	0.99	Hα + 24 μm
Medling et al. (2018)	1.00	Hα
Cano-Díaz et al. (2019)	0.94	Hα
Bluck et al. (2019)	0.90	Hα
This work	0.82	SED fitting

however, might prevent a comprehensive evaluation of the energetic budget in galaxies, as UV and optical tracers could underestimate a fraction of the obscured SFR (e.g. Rodighiero et al. 2014). In this section, we thus compare our panchromatic results with the spatially resolved MS relations obtained with data from CALIFA (Cano-Díaz et al. 2016), MaNGA (Hsieh et al. 2017; Bluck et al. 2019; Cano-Díaz et al. 2019), and SAMI (Medling et al. 2018). For completeness, we also compare our results with the MS relations of Abdurro'uf (2017), who performs pixel-by-pixel SED fitting to *GALEX* and SDSS photometry of local ($0.01 < z < 0.02$) massive spiral galaxies selected in the MPI-JHU (Max Planck Institute for Astrophysics-Johns Hopkins University), and of Hall et al. (2018), obtained for a sample of 355 nearby galaxies, with spatially resolved observations of Hα and mid-IR emission.

In Fig. 8 we show the spatially resolved MS relation of this work (solid black line) together with the relations mentioned above. To underline the depth of each study, in Fig. 8 we plot the relations as starting from the $\log M_\star$ value above which 80 per cent of the corresponding data are located. The relations have been homogenized in terms of IMF and cosmology, and rescaled to the median redshift of our sample, using the evolution in MS normalization of SFR $\propto (1+z)^{2.88}$ (Whitaker et al. 2014).

The spatially resolved MS of Cano-Díaz et al. (2016, lavender dashed line) has been estimated from a sample of 306 galaxies with mixed morphologies at $0.005 < z < 0.03$, on spatial scales of 0.5–1.5 kpc. They find a slope of 0.72. Similarly, Hsieh et al. (2017) used 536 SFGs at $0.01 < z < 0.15$ from the MaNGA survey to obtain an MS relation on scales of ∼1 kpc (green dash–dotted line), obtaining a slope of 1.00 with the ODR fitting method. Recently, Cano-Díaz et al. (2019) updated the work of Hsieh et al. (2017) using ∼2000 galaxies from the MaNGA MPL-5 release ($0.01 < z < 0.15$) to probe the spatially resolved MS for a larger sample, again on spatial scales of ∼1.0 kpc. Their MS relation (orange dash–dotted line) has a slope of 0.94. Based on ∼3500 local galaxies in the SDSS-IV MaNGA-DR15 data, with SFRs coming from D4000 and Hα observations whenever available, Bluck et al. (2019, yellow line) obtain a slope of 0.90 on a data set of over 5 million spaxels. Maragkoudakis et al. (2017, blue dotted line) evaluate SFRs from IRAC 3.6 and 8.0 μm data at sub-kpc scales on a sample of 369 nearby galaxies ($z \sim 0.02$), obtaining a slope of 0.91. The MS of Medling et al. (2018, purple solid line) has been estimated from ∼800 galaxies in the SAMI Galaxy Survey at $z < 0.1$ and has a slope of 1.0. The MS relation of Hall et al. (2018, magenta dashed line) has a slope of 0.99, and was computed exploiting spatially resolved Hα observations of nearby galaxies within the Survey of Ionization in Neutral Gas Galaxies (SINGG) and WISE surveys (we report here the relation obtained using the SFR transformation of Calzetti et al. 2007). Finally, the MS of Abdurro'uf (2017, red line) has a slope of 0.99. All the reported spatially resolved MS slopes are reported in Table 2.

The immediate take-home information evident from Fig. 8 is that thanks to our multiwavelength approach we are able to probe regions of lower stellar mass surface densities (up to a factor of 10) compared to spectroscopic observations, bound to the sensitivity limit of the Hα line. This translates in the ability of sampling regions that are located further away from the galaxy centre, up to ∼2.5–3 effective radii (Re). While it is true that CALIFA galaxies have been selected in size so that most of them are fully sampled by the instrument field of view, the requirement to observe the Hα line with an SNR (S/N) > 3 in each resolution element translates in smaller radii within which the SFR can be efficiently computed, as it is clear from the different sensitivity limit. The same reasoning applies to the MS relations of Medling et al. (2018) and Cano-Díaz et al. (2019). On the other hand, Hall et al. (2018) reach lower $\Sigma_{\rm SFR}$ thanks to the combination of Hα and mid-IR data, but it has the drawback that low $\Sigma_{\rm SFR}$ only traces obscured SF.

The MS slope that we obtain is lower than the ones shown in Fig. 8 with the exception of the Cano-Díaz et al. (2016) relation. To exclude effects due to different fitting procedures, which can largely affect the MS slope and intercept, we also compute the relation using the ODR method, and we find a slope of 0.88. This value is still lower than the ones found in the works mentioned above, but it is important to underline that our relation was computed from eight galaxies against the hundreds of sources of other works. As there are strong galaxy-to-galaxy variations, it is important to apply our approach on a larger sample to carry out a more meaningful comparison with other works.

5 DISCUSSION AND CONCLUSIONS

In this paper, we have presented a new analysis of eight local face-on spirals, with the aim of understanding if the MS is a universal

relation holding also on sub-galactic scales. Other surveys of nearby galaxies have addressed this question, showing clear correlation between stellar masses and star formation per unit area, and to their gas content (Bigiel et al. 2008; Leroy et al. 2008; Casasola et al. 2015). By exploiting the publicly available photometric information of DustPedia in the UV-to-FIR spectral range, we have been able to perform a global SED fitting procedure that allowed us to simultaneously account for a careful evaluation of the obscured and unobscured SFR components, over the full optical radius, larger than what is obtained with optical IFS at similar redshifts. Our limited sample is restricted to the grand-design spirals with low inclination, large spatial extension, and regular spiral arm structures in DustPedia. This analysis has provided a total of tens of thousands of physical cells on typical scales of ∼0.5 kpc over very different internal galaxy environments (bulges, spiral arms, inter-arms regions, and outskirts). This set is thus well fit to study the secular evolution processes that regulate the star formation in local sources, dominated by rotationally supported systems (e.g. Förster Schreiber et al. 2009; Law et al. 2009; Glazebrook 2013; Wisnioski et al. 2015; Simons et al. 2017; Förster Schreiber et al. 2018; Übler et al. 2019).

Some individual galaxies show peculiar variation around the Σ_{SFR}–$\Sigma_{\star}$ relation presented in Fig. 6 (see the bottom right panels in Figs A1–A7). For example, NGC 3938 and NGC 4254 show an average enhancement of the SFR, which we interpret as a possible effect of the environment, as these two sources are located in the Ursa Major group and the Virgo cluster, respectively. Other galaxies, in particular NGC 0628, show a prominent bulge feature appearing as a narrow distribution at the highest stellar mass densities. Indeed, we already mentioned that at the lowest stellar mass densities (i.e. at large galactocentric distances) in few sources we have identified a cloud of cells deviating from the main relation towards lower SFR, at a fixed stellar mass (NGC 4321 is the cleanest example). Such distributions are circularly distributed in the outer parts of the galaxies, out of the regions spanned by the dynamical interaction of the spiral arms. It is still to be understood if this is associated with an older population migrated out of the disc, or if it is the remnant of external accretion through, for example, minor merging. Finally, only NGC 5457 reveals strong mini-starbursts inside the spiral arms (i.e. regions well elevated above the MS, by a factor larger than 10–100 times at a fixed mass density).

In any case, the combination of all the eight galaxies demonstrates the existence of a universal relation, as the deviation of single sources is well within the global scatter of ∼0.27 dex (see Section 4.3). We have then demonstrated that such a relation holds at different galaxy scales, supporting the interpretation from other surveys that the SFR is regulated by local processes of gas-to-stars conversion happening at GMC scales of the order of a few hundred pc. With respect to other works, we have, however, provided evidence that such *secular regulation* keeps to apply at the farthest galactocentric distances, where the optical disc is still influenced by the density wave motions, originating the spiral arms.

This work defines an accurate locus in the Σ_{SFR}–$\Sigma_{\star}$ plane, constrained by observed distributions covering 3 dex in the parameter space. Such a definition of the spatially resolved MS in local disc galaxies represents a valuable reference for future comparison to different galaxy morphological types adopting a similar panchromatic approach. Indeed, there are indications that galaxy morphology plays an important role in characterizing the spatially resolved MS relation, especially its scatter (e.g. González Delgado et al. 2016; Cano-Díaz et al. 2019). Maragkoudakis et al. (2017) observe a decrease in the spatially resolved MS relation from late-type to early-type spirals, while the scatter remains constant. Other works do not find a similar connection (Hall et al. 2018). These examples show the importance of extending the analysis performed in this work to a larger sample of galaxies encompassing different morphologies.

In the second paper of this series, we will exploit this reference sample to study if and how the distance to the resolved MS is connected to the total (atomic and molecular) gas content (Morselli et al., in prep.).

6 SUMMARY

The star-forming MS is a well-studied tight relation between stellar masses and SFRs, observed up to $z \sim 6$, over a great variety of environments and morphologies, both globally, counting galaxies as a whole, and locally, resolving physical properties in single galaxy regions. In this work, we perform spatially resolved SED fitting in a sample of eight local grand-design spirals taken from the DustPedia archive and we use the outputted maps of stellar mass and SFR (see the appendix) to analyse the spatially resolved MS of SFGs on scales spanning the range between 0.4 and 1.5 kpc. We summarize here our main findings:

(i) When considering the eight galaxies together, we obtain a spatially resolved MS with a slope of 0.82 and an intercept of −8.69. When fitting the data with the ODR method, we obtain a slope and an intercept of 0.88 and −9.05, respectively. This relation holds on different scales, from sub-galactic to galactic;

(ii) The local spatially resolved MS is consistent with the evolutionary (from high-z) low-mass relation, thus proving its universality across cosmic time. This is a crucial point to validate the integrated information on individual galaxies at high redshifts;

(iii) We have overtaken the limits of all the spectroscopic resolved emission line studies, based mainly on Hα and Balmer decrement corrections for dust extinction. The sensitivities of these surveys do not sample the lowest $M_{\star}$ and SFR as we do with a multiwavelength photometric approach, allowing us to probe the outermost regions of galaxies.

We plan to extend this analysis on different morphological types inside the DustPedia sample, while improving the SED fitting pipeline to investigate star formation histories of resolved galaxy regions. We will also link these results with existing gas observations (i.e. CO, H_2, and C II) to further understand the role of secular evolution in galaxies.

ACKNOWLEDGEMENTS

We would like to thank the anonymous referee for the useful comments improving the overall work quality. We are grateful to CJR Clark for the information on CAAPR, and to M. Cano-Diaz for providing us the CALIFA results from her 2016 paper. AE and GR are supported from the STARS@UniPD grant. GR acknowledges the support from grant PRIN MIUR 2017 – 20173ML3WW_001. GR and CM acknowledge funding from the INAF PRIN-SKA 2017 programme 1.05.01.88.04. We acknowledge funding from the INAF main stream 2018 programme 'Gas-DustPedia: A definitive view of the ISM in the Local Universe'. This research is based on observations made with the *GALEX*, obtained from the MAST data archive at the Space Telescope Science Institute, which is operated by the Association of Universities for Research in Astronomy, Inc., under NASA contract NASA 5-26555. DustPedia is a collaborative focused research project supported by the European Union under the Seventh Framework Programme (2007–2013) call (proposal no. 606847). The participating institutions are as follows: Cardiff University, UK; National Observatory of Athens, Greece;

Ghent University, Belgium; Université Paris Sud, France; National Institute for Astrophysics, Italy and CEA (Paris), France. We acknowledge the usage of the HyperLeda database (http://leda.univ-lyon1.fr). This research made use of PHOTUTILS, an Astropy package for the detection and photometry of astronomical sources.

REFERENCES

Abdurro'uf A. M., 2017, MNRAS, 469, 2806
Abdurro'uf A. M., 2018, MNRAS, 479, 5083
Aniano G., Draine B. T., Gordon K. D., Sandstrom K., 2011, PASP, 123, 1218
Bell E. F., Kennicutt R. C., Jr, 2001, ApJ, 548, 681
Berta S. et al., 2013, A&A, 551, A100
Bigiel F., Leroy A., Walter F., Brinks E., de Blok W. J. G., Madore B., Thornley M. D., 2008, AJ, 136, 2846
Bluck A. F. L., Maiolino R., Sánchez S. F., Ellison S. L., Thorp M. D., Piotrowska J. M., Teimoorinia H., Bundy K. A., 2019, MNRAS, 485, 2839
Bradley L. et al., 2019, Astropy/photutils: v0.6. available at: https://doi.org/10.5281/zenodo.2533376
Brammer G. B. et al., 2012, ApJS, 200, 13
Bruzual G., Charlot S., 2003, MNRAS, 344, 1000
Bundy K. et al., 2015, ApJ, 798, 7
Calzetti D. et al., 2007, ApJ, 666, 870
Camps P., Baes M., 2015, Astron. Comput., 9, 20
Cano-Díaz M. et al., 2016, ApJ, 821, L26
Cano-Díaz M., Ávila-Reese V., Sánchez S. F., Hernández-Toledo H. M., Rodríguez-Puebla A., Boquien M., Ibarra-Medel H., 2019, MNRAS, 488, 3929
Casasola V., Hunt L., Combes F., García-Burillo S., 2015, A&A, 577, A135
Chabrier G., 2003, PASP, 115, 763
Chang Y.-Y., van der Wel A., da Cunha E., Rix H.-W., 2015, ApJS, 219, 8
Charlot S., Fall S. M., 2000, ApJ, 539, 718
Chevance M. et al., 2019, MNRAS, in press
Chrimes A. A., Stanway E. R., Levan A. J., Davies L. J. M., Angus C. R., Greis S. M. L., 2018, MNRAS, 478, 2
Clark C. J. R. et al., 2018, A&A, 609, A37
Conselice C. J., Wilkinson A., Duncan K., Mortlock A., 2016, ApJ, 830, 83
Corwin Harold G. J., Buta R. J., de Vaucouleurs G., 1994, AJ, 108, 2128
Croom S. M. et al., 2012, MNRAS, 421, 872
da Cunha E., Charlot S., Elbaz D., 2008, MNRAS, 388, 1595
da Cunha E., Charmandaris V., Díaz-Santos T., Armus L., Marshall J. A., Elbaz D., 2010, A&A, 523, A78
Daddi E. et al., 2007, ApJ, 670, 156
Davies J. I. et al., 2017, PASP, 129, 044102
0000000de Vaucouleurs G., de Vaucouleurs A., Corwin Herold G. J., Buta R. J., Paturel G., Fouque P., 1991, Third Reference Catalogue of Bright Galaxies, Vol. 82, Sky and Telescope, p. 621
Driver S. P. et al., 2018, MNRAS, 475, 2891
Elbaz D. et al., 2007, A&A, 468, 33
Foreman-Mackey D., Hogg D. W., Lang D., Goodman J., 2013, PASP, 125, 306
Förster Schreiber N. M. et al., 2009, ApJ, 706, 1364
Förster Schreiber N. M. et al., 2018, ApJS, 238, 21
Glazebrook K., 2013, Publ. Astron. Soc. Aust., 30, e056
González Delgado R. M. et al., 2016, A&A, 590, A44
Grogin N. A. et al., 2011, ApJS, 197, 35
Hall C., Courteau S., Jarrett T., Cluver M., Meurer G., Carignan C., Audcent-Ross F., 2018, ApJ, 865, 154
Hayward C. C., Smith D. J. B., 2015, MNRAS, 446, 1512
Hemmati S. et al., 2014, ApJ, 797, 108
Hsieh B. C. et al., 2017, ApJ, 851, L24
Jafariyazani M., Mobasher B., Hemmati S., Fetherolf T., Khostovan A. A., Chartab N., 2019, ApJ, 887, 204
Kennicutt R. C., Jr, 1998, ApJ, 498, 541
Khoperskov S. A., Vasiliev E. O., 2017, MNRAS, 468, 920
Koekemoer A. M. et al., 2011, ApJS, 197, 36
Kravtsov A. V., 2003, ApJ, 590, L1
Law D. R., Steidel C. C., Erb D. K., Larkin J. E., Pettini M., Shapley A. E., Wright S. A., 2009, ApJ, 697, 2057
Leroy A. K., Walter F., Brinks E., Bigiel F., de Blok W. J. G., Madore B., Thornley M. D., 2008, AJ, 136, 2782
Lin L. et al., 2017, ApJ, 851, 18
Magdis G. E. et al., 2016, MNRAS, 456, 4533
Makarov D., Prugniel P., Terekhova N., Courtois H., Vauglin I., 2014, A&A, 570, A13
Maragkoudakis A., Zezas A., Ashby M. L. N., Willner S. P., 2017, MNRAS, 466, 1192
Martis N. S., Marchesini D. M., Muzzin A., Stefanon M., Brammer G., da Cunha E., Sajina A., Labbe I., 2019, ApJ, 882, 65
Medling A. M. et al., 2018, MNRAS, 475, 5194
Meurer G. R. et al., 2006, ApJS, 165, 307
Morrissey P. et al., 2007, ApJS, 173, 682
Morselli L., Popesso P., Erfanianfar G., Concas A., 2017, A&A, 597, A97
Noeske K. G. et al., 2007, ApJ, 660, L47
Oliver S. et al., 2010, MNRAS, 405, 2279
Pannella M. et al., 2009, ApJ, 698, L116
Pearson W. J. et al., 2018, A&A, 615, A146
Peng Y., Maiolino R., Cochrane R., 2015, Nature, 521, 192
Pérez E. et al., 2013, ApJ, 764, L1
Pilbratt G. L. et al., 2010, A&A, 518, L1
Planck Collaboration XIII, 2016, A&A, 594, A13
Poggianti B. M. et al., 2017, ApJ, 844, 48
Popesso P. et al., 2019a, MNRAS, 483, 3213
Popesso P. et al., 2019b, MNRAS, 490, 5285
Renzini A., Peng Y.-j., 2015, ApJ, 801, L29
Rodighiero G. et al., 2011, ApJ, 739, L40
Rodighiero G. et al., 2014, MNRAS, 443, 19
Rosales-Ortega F. F., Sánchez S. F., Iglesias-Páramo J., Díaz A. I., Vílchez J. M., Bland-Hawthorn J., Husemann B., Mast D., 2012, ApJ, 756, L31
Saintonge A. et al., 2016, MNRAS, 462, 1749
Sánchez S. F. et al., 2012, A&A, 538, A8
Sánchez S. F. et al., 2013, A&A, 554, A58
Sánchez S. F., 2019, preprint (arXiv:1911.06925)
Santini P. et al., 2009, A&A, 504, 751
Santini P. et al., 2017, ApJ, 847, 76
Sargent M. T., Bethermin M., Daddi E., Elbaz D., 2012, ApJ, 747, L31
Schreiber C. et al., 2015, A&A, 575, A74
Schruba A., Leroy A. K., Walter F., Sand strom K., Rosolowsky E., 2010, ApJ, 722, 1699
Shivaei I., Reddy N. A., Steidel C. C., Shapley A. E., 2015, ApJ, 804, 149
Simons R. C. et al., 2017, ApJ, 843, 46
Skrutskie M. F. et al., 2006, AJ, 131, 1163
Smith D. J. B., Hayward C. C., 2015, MNRAS, 453, 1597
Smith D. J. B., Hayward C. C., 2018, MNRAS, 476, 1705
Smith D. J. B. et al., 2012, MNRAS, 427, 703
Sobral D., Best P. N., Smail I., Mobasher B., Stott J., Nisbet D., 2014, MNRAS, 437, 3516
Solomon P. M., Rivolo A. R., Barrett J., Yahil A., 1987, ApJ, 319, 730
Speagle J. S., Steinhardt C. L., Capak P. L., Silverman J. D., 2014, ApJS, 214, 15
Steinhardt C. L. et al., 2014, ApJ, 791, L25
Tacchella S., Dekel A., Carollo C. M., Ceverino D., DeGraf C., Lapiner S., Mandelker N., Primack J. R., MNRAS, 2016, 458, 242
Viaene S. et al., 2014, A&A, 567, A71
Vulcani B. et al., 2019, MNRAS, 488, 1597
Werner M. W. et al., 2004, ApJS, 154, 1
Whitaker K. E. et al., 2014, ApJ, 795, 104
Williams T. G., Gear W. K., Smith M. W. L., 2018, MNRAS, 479, 297
Wisnioski E. et al., 2015, ApJ, 799, 209
Wright E. L. et al., 2010, AJ, 140, 1868
Wuyts S.et al.,2011, ApJ, 742, 96
Wuyts S. et al., 2013, ApJ, 779, 135
York D. G. et al., 2000, AJ, 120, 1579
Übler H. et al., 2019, ApJ, 880, 48

APPENDIX A: GALAXY-BY-GALAXY RESULTS

In this appendix, we present the individual galaxy-by-galaxy results, reporting the SFR and stellar mass maps, along with a map measuring the distance from the fitted MS (blue points towards starburst and red points towards quenched ones). In the lower left panel, we report the results on the $M_\star$–SFR plane, with fitted (total) MS in black and the one fitting the lone galaxy results.

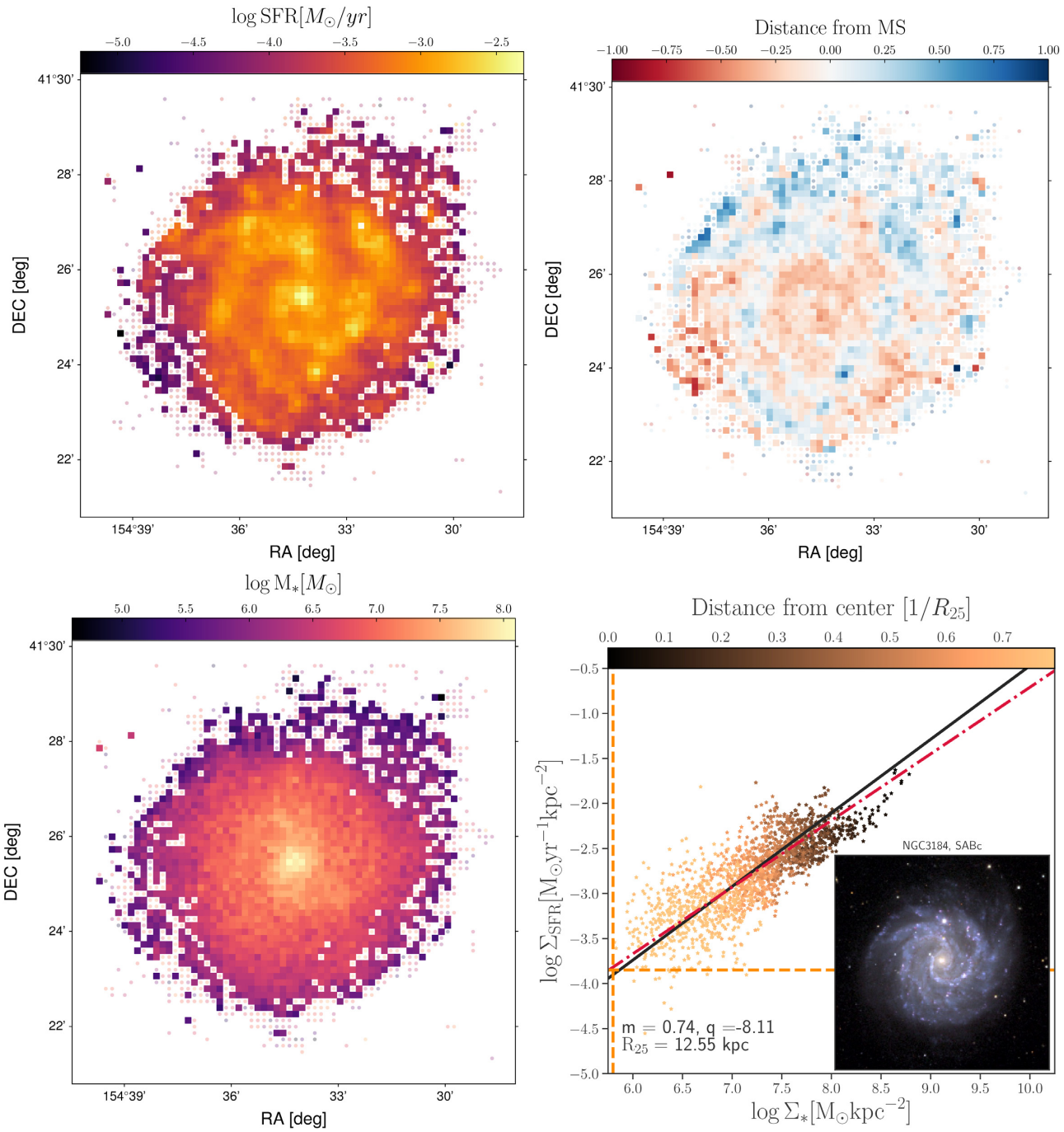

Figure A1. Same as Fig. 4, for NGC 3184.

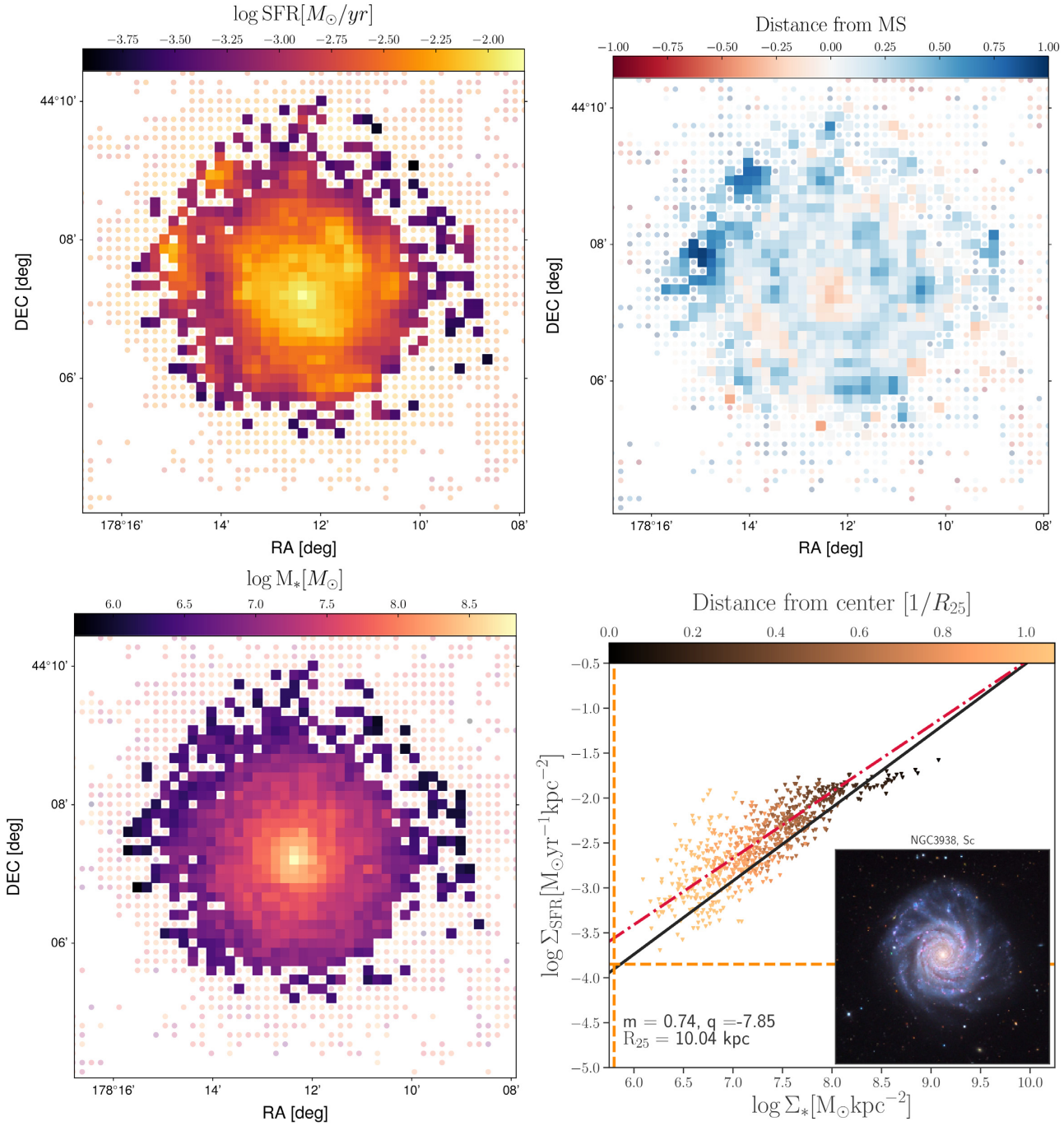

Figure A2. Same as Fig. 4, for NGC 3938.

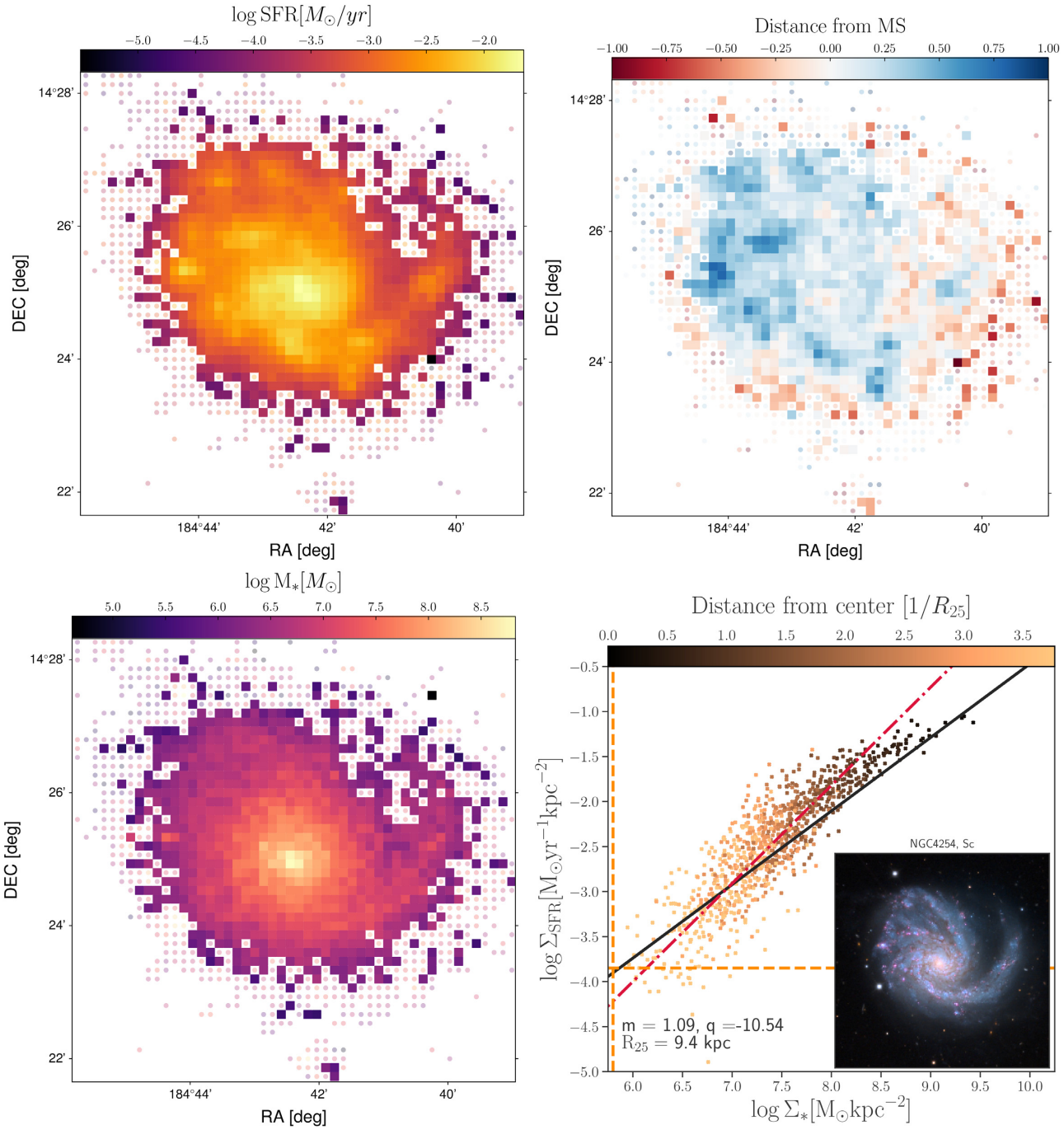

Figure A3. Same as Fig. 4, for NGC 4254.

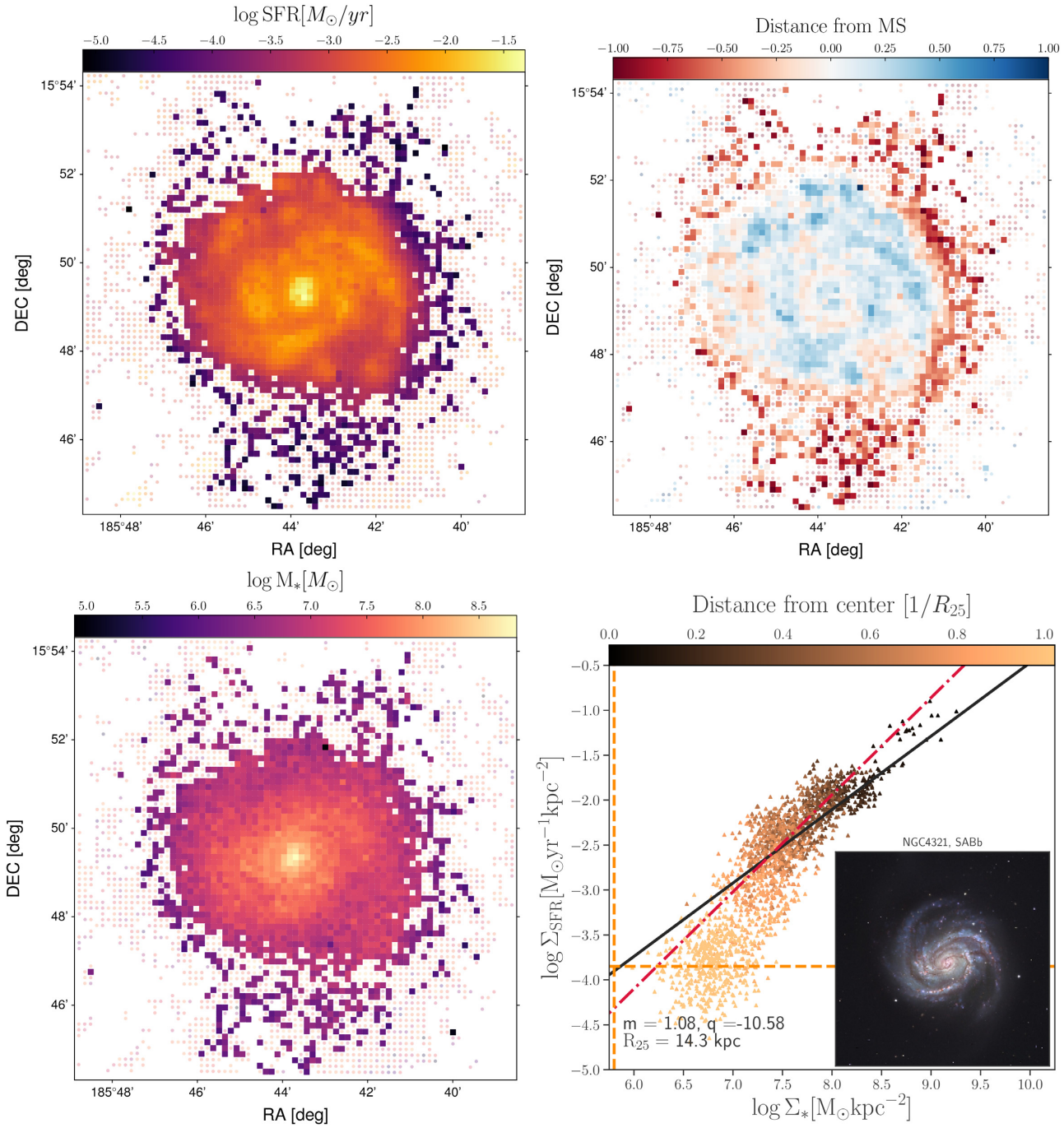

Figure A4. Same as Fig. 4, for NGC 4321.

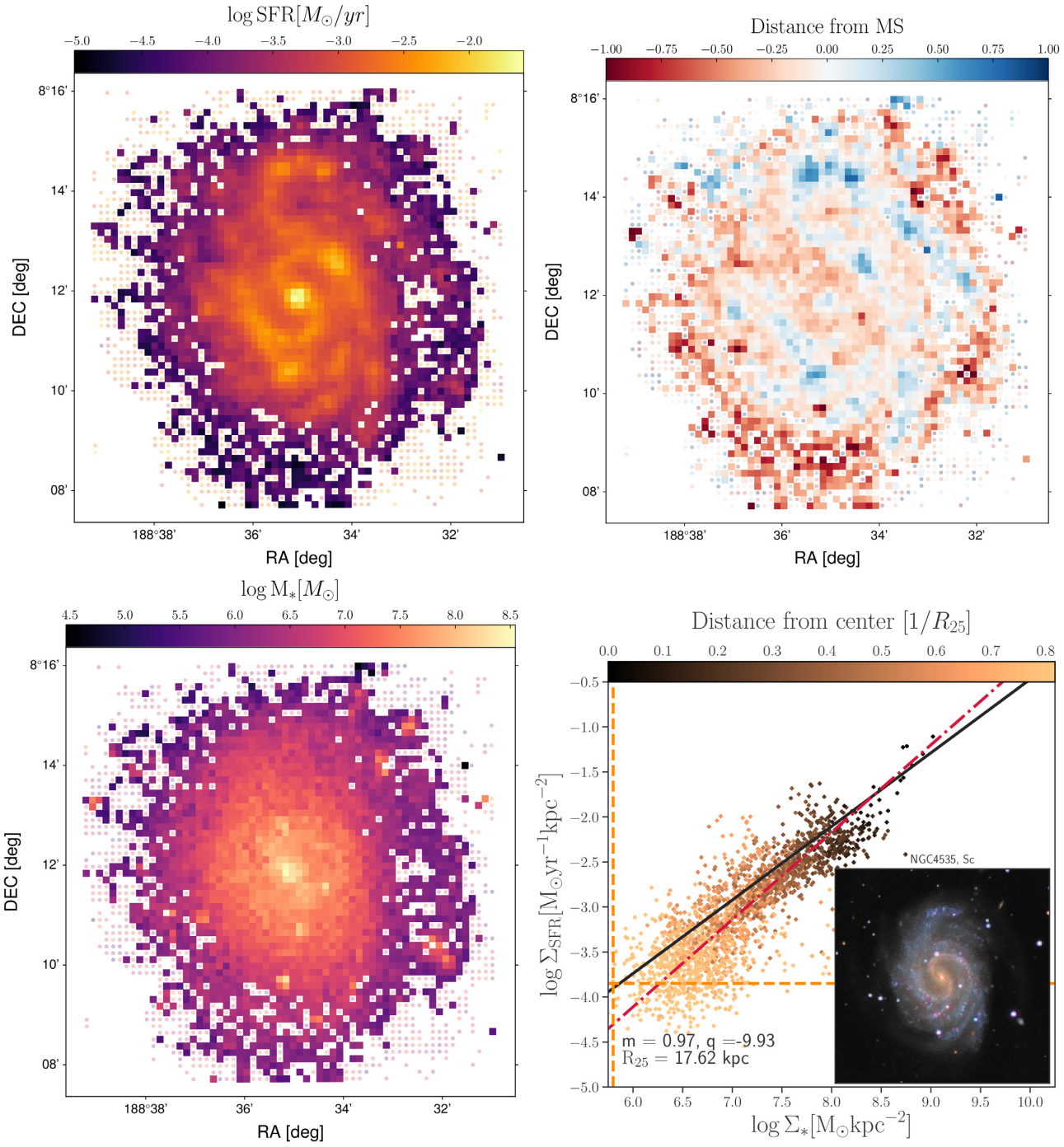

Figure A5. Same as Fig. 4, for NGC 4535.

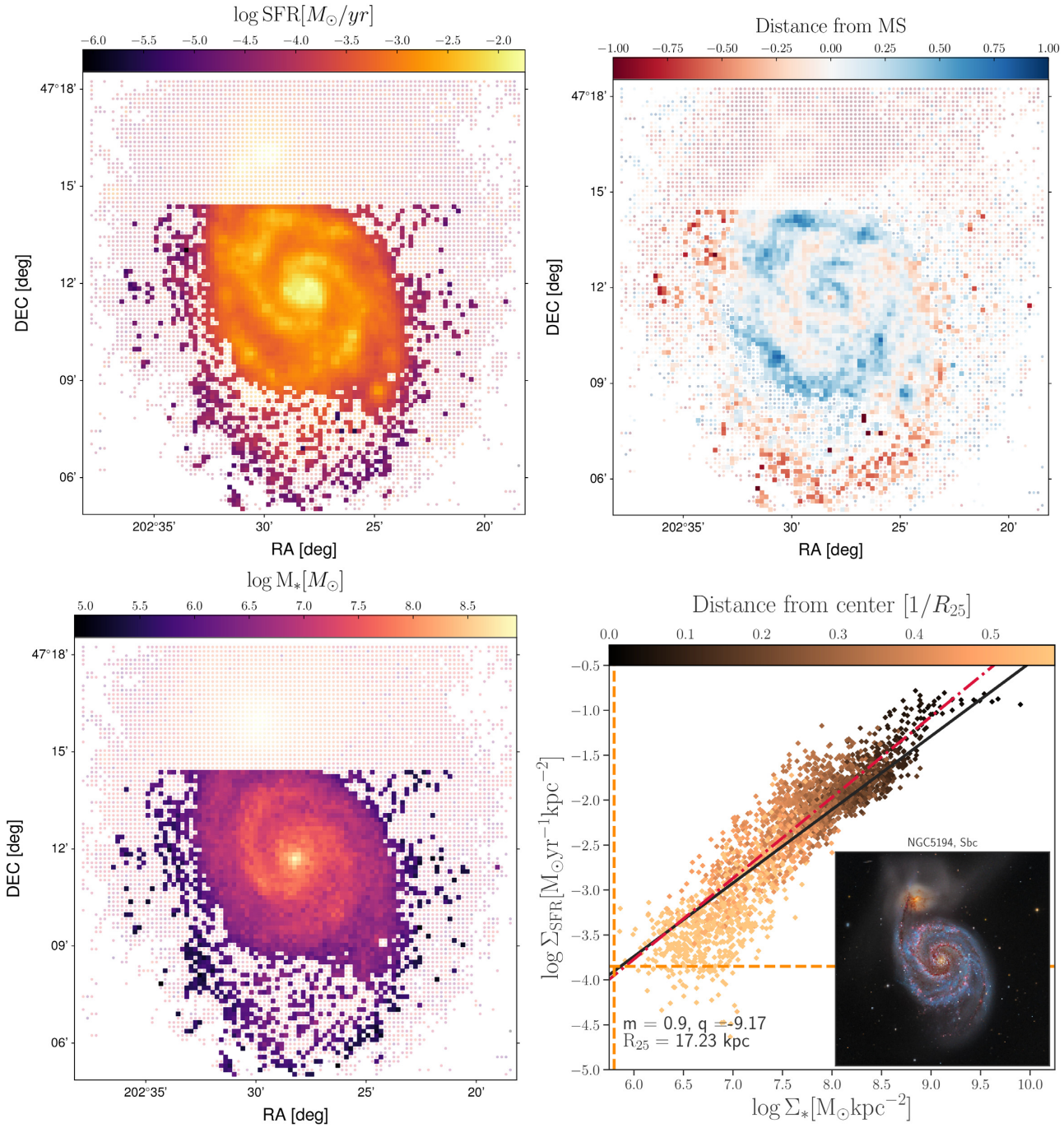

Figure A6. Same as Fig. 4, for NGC 5194.

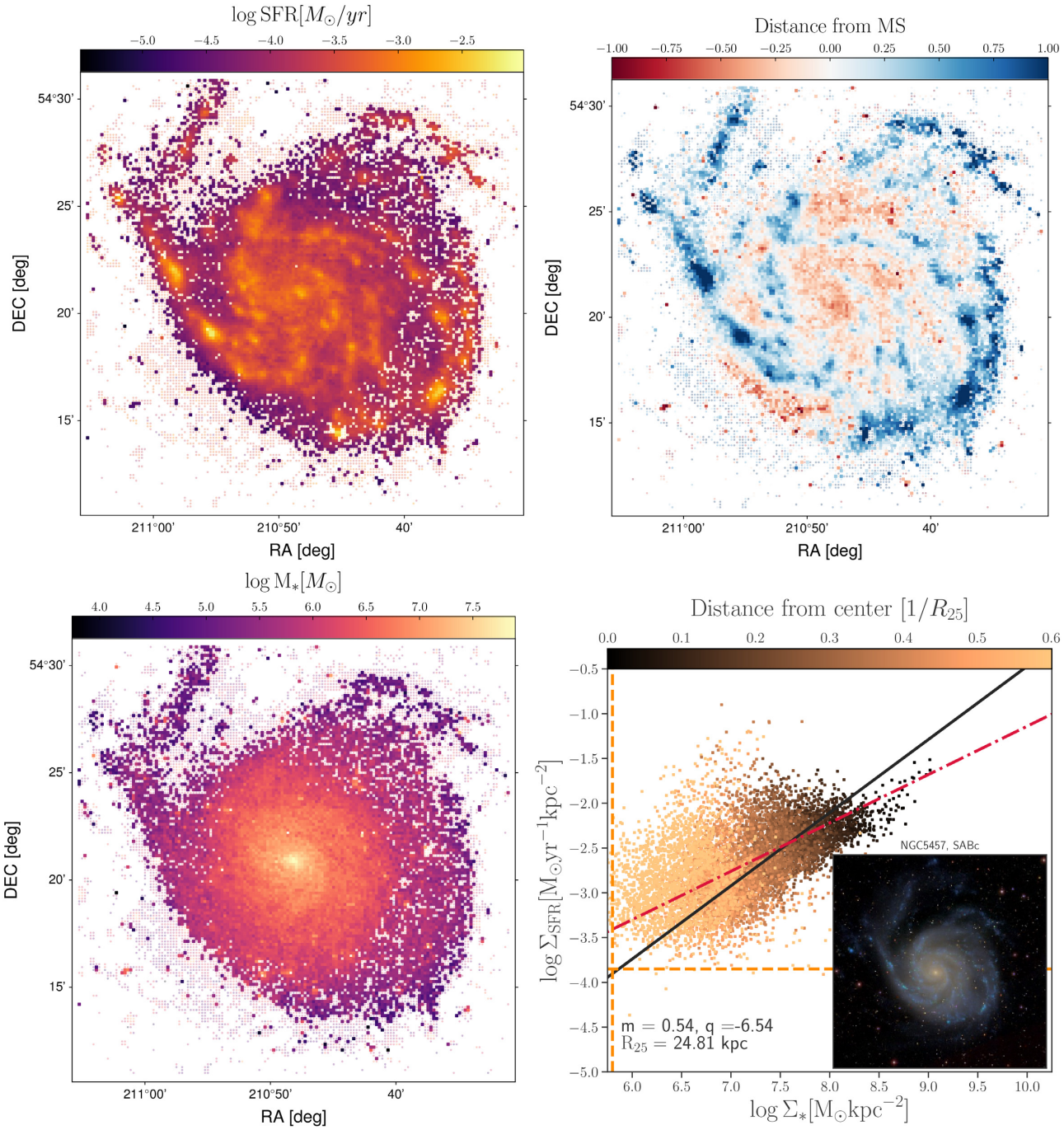

Figure A7. Same as Fig. 4, for NGC 5457.

This paper has been typeset from a TEX/LATEX file prepared by the author.